Observations and Scale Analysis of Coastal Wind Jets

JAMES E. OVERLAND

Pacific Marine Environmental Laboratory/NOAA, Seattle, Washington

NICHOLAS A. BOND

JISAO, University of Washington, Seattle, Washington

(Manuscript received 9 June 1994, in final form 21 February 1995)

ABSTRACT

Blocking of onshore flow by coastal mountains was observed south of Vancouver Island, British Columbia, by the NOAA P-3 aircraft on 1 December 1993. Winds increased from 10 m s^{-1} offshore to 15 m s^{-1} nearshore and became more parallel to shore in the blocked region, which had a vertical scale of 500 m and an offshore scale of 40–50 km. These length scale and velocity increases are comparable to theory. The flow was semi-geostrophic with the coast being hydrodynamically steep; that is, the coast acts like a wall and the alongshore momentum balance is ageostrophic. This is shown by the nondimensional slope parameter—the Burger number, $B = h_m N/fL_m$—being greater than 1, where h_m and L_m are the height and half-width of the mountain, N is the stability frequency, and f is the Coriolis parameter. The height scale is given by setting the local Froude number equal to 1—that is, $h_l = U/N \sim 500$ m, where U is the onshore component of velocity. This scale is appropriate when h_l is less than the mountain height, h_m; in this case $h_l/h_m \sim 0.4$. The offshore scale is given by the Rossby radius $L_R = (Nh_m/f)F_m = U/f \sim 50$ km for $F_m < 1$, where the mountain Froude number $F_m = h_l/h_m = U/h_m N \sim 0.4$. The increase in the alongshore wind speed due to blocking, ΔV, is equal to the onshore component of the flow, $U \approx 6$ m s^{-1} or in this case about half of the near-coastal alongshore component. A second case on 11 December 1993 had stronger onshore winds and weak stratification and was in a different hydrodynamic regime, with $F_m \sim 6$. When $F_m > 1$, $L_R = Nh_m/f \sim 200$ km, and $\Delta V = h_m N \sim 2$ m s^{-1}, a small effect comparable to changes in the synoptic-scale flow. The authors expect a maximum coastal jet response when $F_m \sim 1$.

1. Introduction

A turning of the wind velocity to be more parallel to the shore, often accompanied by a change in speed, is a ubiquitous phenomena for onshore stratified flow near mountainous coasts. The phenomenon is often called windward ridging or blocking. Examples come from southwest Alaska (Lackmann and Overland 1989), Washington State (Mass and Ferber 1990), and southeast Norway (Økland 1990). In some cases, the terrain-induced pressure perturbations cause enhanced coastal wind speeds (e.g., Overland and Bond 1993). Key issues are to understand which parameters control the seaward and vertical extent of the modification of wind speed and direction and what parameters control the magnitude of the response. Atmospheric stability large enough to induce blocking often occurs in prefrontal air masses over the northeast Pacific Ocean and is generally associated with postfrontal conditions over continental regions such as north of the Alps (Chen and Smith 1987) or the west slopes of the Sierra Nevada (Parish 1982) and Rocky Mountains.

As part of the Coastal Observation and Simulation with Topography (COAST) field program, a NOAA P-3 research aircraft collected extensive low-level observations on the southern side of Vancouver Island on 1 December 1993 during a period of relatively steady-state onshore-directed flow. These observations are used to document a case of coastal blocking of appealing simplicity. The seaward and vertical extent of the blocked flow is compared with the results of a scale analysis based on a local Froude number. Results are also presented for the 11 December 1993 case from COAST, when the static stability was much lower. Our intent is to show that these two cases of mesoscale structure upwind of terrain lie in different hydrodynamic regimes, where the offshore length scale and coastal wind intensity have a different functional dependence on the stability, onshore wind speed component, and mountain height. Rather than conduct detailed numerical case studies, we present scaling arguments and use the observational base to distinguish the two hydrodynamical regimes based on what we term a mountain Froude number, F_m.

Corresponding author address: Dr. James E. Overland, Pacific Marine Environmental Laboratory, NOAA, Building No. 3, 7600 Sand Point Way, N.E., Seattle, WA 98115.

The scale analyses follows Pierrehumbert and Wyman (1985), Bannon and Chu (1988), Overland (1984), and Overland and Bond (1993). A basic parameter is the Burger number or dynamically scaled mountain slope

$$B = \left(\frac{h_m}{L_m}\right)\left(\frac{N}{f}\right), \qquad (1)$$

where h_m is the mountain height, L_m is the mountain half-width, N is static stability, and f is the Coriolis force. For $B \ll 1$ the flow is quasigeostrophic as the flow proceeds over the mountain. If $0.1 \leq B \leq 1.0$, the solution for the mountain influence is semigeostrophic and depends only on the value of B (Pierrehumbert and Wyman 1985; see their Fig. 14). Here the wind field is modified by the slope of the mountain, primarily over the mountain. If $B > 1$ the mountain is hydrodynamically steep, blocking is complete, and the influence of the mountain is independent of the mountain half-width (Overland and Bond 1993). In our 1 December Vancouver Island case the flow is in the steep regime, $B > 1$, and the incident flow is weak enough that the mountain height also is not a scaling parameter. It bears emphasizing that scale analysis is based on order of magnitude assumptions. In this paper we do not address details caused by the variations in the actual topography nor directly the temporal evolution of the blocked flow (Pierrehumbert and Wyman 1985; Overland and Bond 1993).

2. Case of 1 December 1993

a. Synoptic overview

The flight observations were conducted between about 2200 UTC 30 November and 0200 UTC 1 December 1993 in the vicinity of 49°N, 126.5°W off the southwestern coast of Vancouver Island. The 850-mb analysis from the National Meteorological Center (NMC) at 0000 UTC 1 December (Fig. 1) shows a prominent trough over the northeast Pacific Ocean. Strong zonal flow is indicated between 40° and 50°N west of 130°W, and moderate southwesterly flow is indicated over Vancouver Island. The 850-mb wind speeds at Quillayute, Washington (UIL), and Port Hardy, British Columbia (YZT), were 8 and 10 m s^{-1}, respectively. Warm-air advection is shown in the southwesterly flow impinging on the Pacific Northwest coast. This warm-air advection was apparently accompanied and largely counteracted by cooling due to lifting; the 850-mb temperatures at UIL and YZT warmed only about 3° and 1°C, respectively, between 0000 and 1200 UTC 1 December. The 850-mb wind speeds increased by approximately 2–3 m s^{-1} over the same period. The surface analysis for 0000 UTC 1 December from NMC (not shown) indicates a weak warm front extending along 131°W about 500-km southwest of

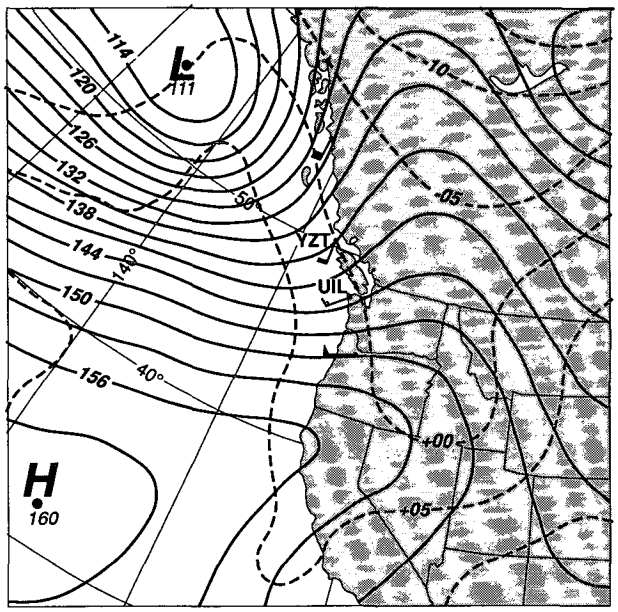

FIG. 1. The 850-mb geopotential height and temperature analysis at 0000 UTC 1 December 1993 from NMC. Selected winds from coastal stations are also shown. Longitudes are every 10°.

Vancouver Island. The surface reports from coastal stations and nearshore buoys in the vicinity of the flight measurements indicated pressure falls of 0–2 mb, wind speed changes of 0–5 m s^{-1}, and near-constant wind directions over the duration of the flight operations. A GOES IR satellite image for 2331 UTC 30 November (Fig. 2) shows a southwest–northeast-oriented cloud band over and upstream of Vancouver Island. Precipitation accompanied this feature; light rain was observed along the coasts of Vancouver Island and Washington State beginning about 0100 UTC.

Even though there were some temporal evolutions, we submit that the large-scale forcing by the background flow was essentially steady state. This assumption allows use of the flight observations to construct a nearly steady picture of the mesoscale structure of the onshore flow on the windward side of Vancouver Island.

b. Mesoscale structure

The first portion of the flight (from 2230 to 0000 UTC) was devoted to mapping the sea level pressure and low-level wind fields. A horizontal map of winds at about 100 m, sea level pressure from aircraft pressure and altitude measurements, and surface reports (Fig. 3) show a distinct transition between southerly winds offshore and southeasterly winds nearshore parallel to the coastal terrain. There was an enhancement of the wind speeds along the coast as well, with typical values of approximately 15 m s^{-1} as compared with 10 m s^{-1}

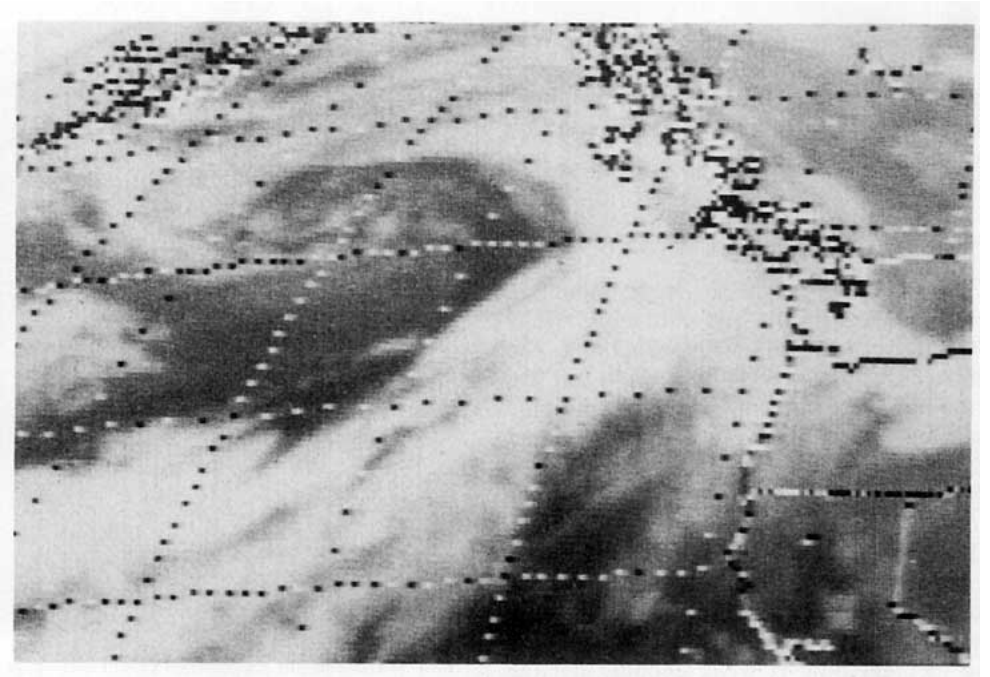

FIG. 2. GOES IR satellite image for 2331 UTC 30 November.

farther offshore. There was good agreement between the surface winds and those from the aircraft, considering that the surface winds would be expected to be somewhat more ageostrophic down the pressure gradient, especially over land. There was excellent agreement between the winds observed about 40 min apart at the crossing point in the pattern at about 49.3°N, 126.3°W. The sea level pressure analysis suggests that the isobars near the coast were more parallel to the coast within the zone of enhanced wind speeds. The aircraft legs extending seaward of Vancouver Island show that the transition between the wind regimes was abrupt, with a horizontal scale of no more than about 10 km at a distance of 40 km from the coast.

Another view of the windward structure is provided by vertical cross sections of potential temperature θ and the along-barrier component of the wind (Fig. 4) based on flight observations collected along AA' of Fig. 3 from 2340 to 0100 UTC. The enhanced coastal winds shown in the previous map are shown here to extend to about 500 m. Figure 4 also shows that this barrier jet was accompanied by relatively cold temperatures and high static stability. In contrast, near-neutral static stability was observed below 800 m farther offshore. The leading edge of the cold air and stronger winds had a steep slope and resembles a front. The flight crew observed reduced visibilities and fog on the landward side of the transition zone, akin to that commonly observed on the cold side of a warm front. Nevertheless, this transition zone does not represent a traditional warm front. As discussed earlier, the NMC surface analysis had a warm front 500 km to the southwest. In addition, Fig. 4 shows that the warm advection and veering with a height associated with the synoptic flow was predominately above 800 m and to the southwest of the low-level wind shift near the coast.

The colder low-level air along Vancouver Island in the vicinity of the vertical cross section appears to have been in a state of approximate semigeostrophic bal-

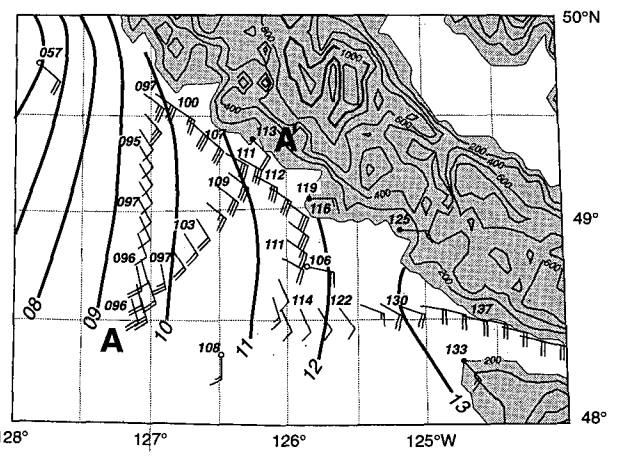

FIG. 3. Map of flight-level winds at approximately 100 m, surface reports over land and water (closed and open circles, respectively), and sea level pressure (solid lines) for the case of 1 December. Selected sea level pressures from aircraft height and pressure measurements are also indicated. The terrain is contoured at 200-m intervals; the 1000-m contour is in bold.

ance. A semiquantitative evaluation of the terms of the momentum equation in the along-barrier direction, assuming steady state, are listed in Table 1. The flow was oriented nearly parallel to the barrier, and the Coriolis force in this direction was negligible. The Lagrangian rate of change of momentum cannot be fully evaluated but appears to have been small. The retarding effect of surface friction was about one-half the magnitude of the acceleration due to the pressure gradient. A substantial portion of the residual is liable to have been due to the retarding effect of vertical entrainment of lower momentum air from above the cold air. Lackmann and Overland (1989) studied a gap flow with similarities to the present case, and found that entrainment and surface friction were of comparable importance in the along-gap momentum balance.

The colder air along Vancouver Island appears to have originated from the Strait of Juan de Fuca and to have had a colder source than the low-level flow farther offshore. The magnitude and depth of the cold air along the coast yields a hydrostatic pressure perturbation of about 0.4 mb, which is comparable to that implied by Fig. 3. Evaporative cooling of this air mass from precipitation aloft was probably of secondary importance since the precipitation observed by the aircraft was light and spotty, and the equivalent potential temperature θ_e of the cold air was approximately 2 K less than that offshore. It does not appear that lifting was responsible for the cooler air, since the flow was parallel to the coast, and its θ was less than that at the surface farther offshore. This value of N used to characterize this case is for the 500-m-deep layer of colder air near the coast.

TABLE 1. Magnitudes of the terms in the along-barrier momentum equation (Overland 1984) for the case of 1 December 1993, evaluated for the colder, low-level air in the vicinity of 49.2°N, 126.4°W.

Term	Magnitude ($\times 10^4$) (m s^{-2})
Pressure gradient (P)	14
Coriolis (C)	~0
Acceleration (A)	~0
Surface friction (F)	7
Residual ($P - C - A - F$)	7

Note that this N is not characteristic of the incident flow, but is rather a reflection of the undercutting cold air. There was an acceleration of this colder air from about 10 m s^{-1} at the west end of the Strait of Juan de Fuca to 15 m s^{-1} at 126°W along Vancouver Island. From mass continuity considerations, this acceleration was accompanied by an unknown combination of shallowing of the cold air and vertical entrainment.

3. Case of 11 December 1993

Flight observations in the vicinity of the coast of Washington State were carried out between about 2100 and 2300 UTC 11 December 1993. Surface reports from stations along the coast indicate a passage of a cold front between 1900 and 2000 UTC. During the 2 h of the flight operations, the surface stations along the coast observed pressure rises of about 2 mb, wind speed increases of 3 m s^{-1}, and little change in wind

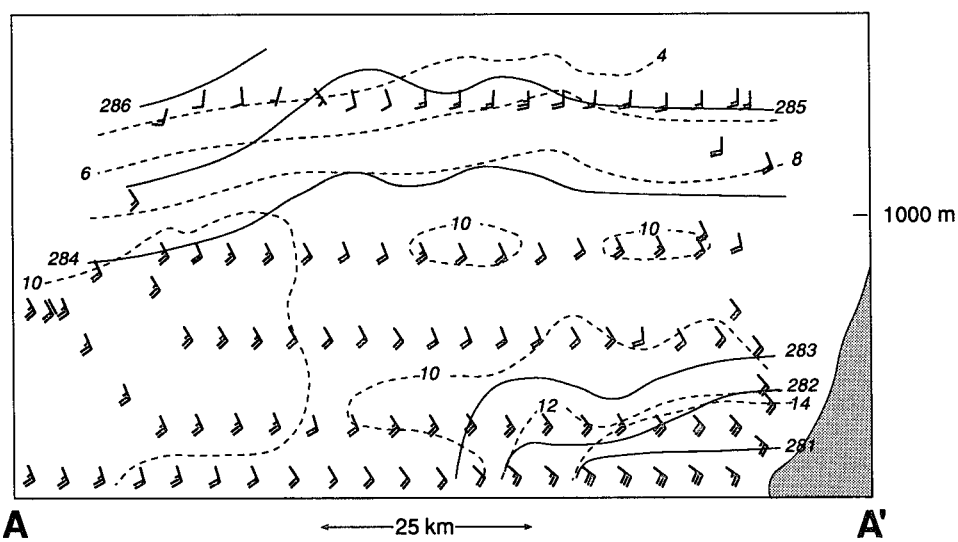

FIG. 4. Vertical cross section along the line AA' of Fig. 3. The solid lines indicate potential temperature (K); the dashed lines indicate the along-barrier component of the wind (m s^{-1}; along 135°). Selected wind barbs are also shown (full barb—5 m s^{-1}). The terrain is indicated with shading. Greatest winds are at low level near the coast.

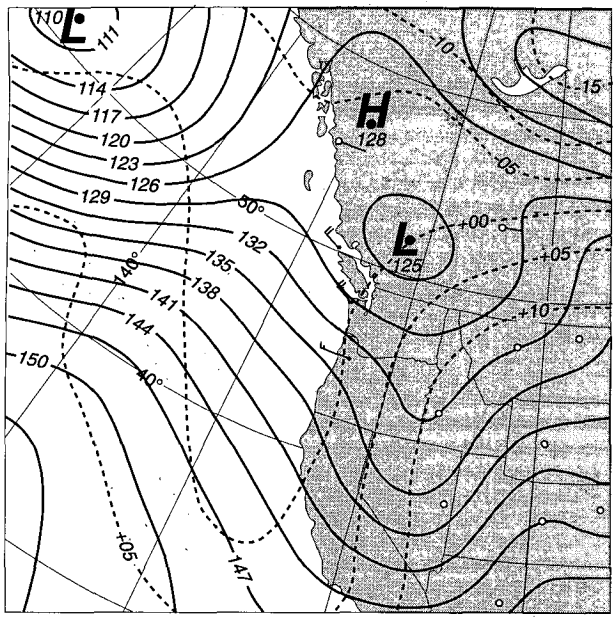

FIG. 5. As in Fig. 1 but for 0000 UTC 12 December 1993.

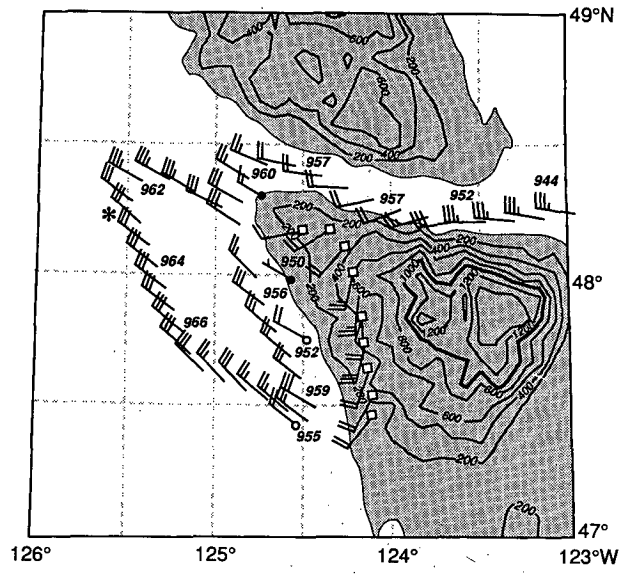

FIG. 6. As in Fig. 3 but for the case of 11 December 1993. The winds with open squares are from flight-level observations at the 1500-m altitude. The star indicates the location of the sounding shown in Fig. 7.

direction. The 850-mb analysis from NMC at 0000 UTC 12 December (Fig. 5) indicates moderate northwesterly flow into the Pacific Northwest within the postfrontal air mass. The satellite imagery at this time shows the open-cell cumulus convection that typically accompanies these cool air masses over the ocean.

A horizontal map of flight-level winds at 100 m, surface reports, and winds at 1500 m on the windward flank of the Olympic Mountains (Fig. 6) shows that the nearshore low-level flow closely resembled that approximately 60 km farther offshore. The wind speeds nearshore averaged about 2 m s^{-1} less than the 15 m s^{-1} speeds found offshore, and the wind directions were virtually uniform. Though the low-level flow near the coast was apparently not significantly affected by the downstream terrain, the winds at the 1500-m level along the terrain were from the south through southwest, and strongly ageostrophic down the synoptic-scale pressure gradient. A sounding at UIL released at about 2000 UTC 11 December (not shown) indicates the frontal zone between 800 and 700 mb; it appears that this leg at 1500 m was just behind this frontal zone. There was channeling and acceleration of the low-level flow through the gap represented by the Strait of Juan de Fuca.

A vertical profile of temperature and dewpoint from flight-level data collected near 48.2°N, 125.6°W at 2230 UTC (Fig. 7) shows that the incident flow had near-neutral static stability and minimal vertical wind shear. The overall N for the layer from 990 to 850 mb (the latter representing the approximate height of the Olympic Mountains) is approximately 7×10^{-3} s^{-1}, assuming saturated processes above 910 mb. Since this profile was collected directly upstream of the coast, and the boundary layer was being warmed and moistened at the sea surface, we contend that the static stability near the coast was also very small. The 0000 UTC 12 December sounding from UIL (not shown) indicates a moist-adiabatic lapse rate except for a thin

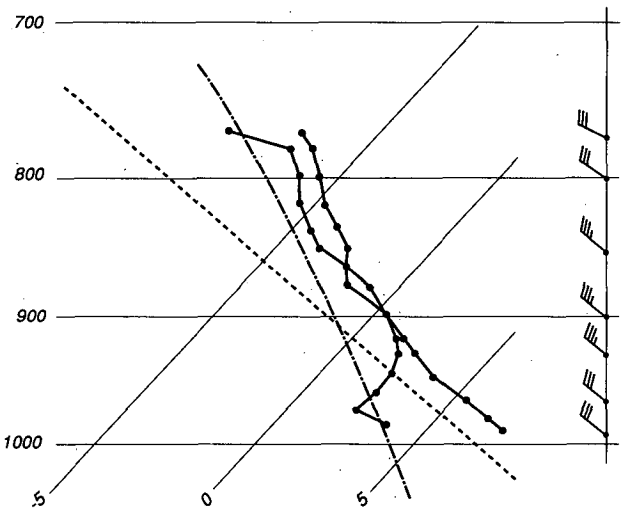

FIG. 7. Skew T–log$p$ profile from the P-3 at approximately 2230 UTC 11 December in the vicinity of 48.2°N, 125.6°W. The dashed line indicates a surface of constant potential temperature; the dash–dotted line indicates a surface of constant equivalent potential temperature.

TABLE 2. Variable definitions.

Variable definition		Variable name	Magnitude Date December 1993	
			1	11
h_m (m)		mountain height	1200	1400
L_m (km)		mountain half-width	40	50
N (s^{-1})	$N^2 = \frac{g}{\theta_0}\frac{\partial\theta}{\partial z}$	static stability, g—gravity, θ—potential temperature	1.3×10^{-2}	1.5×10^{-3}
U (m s^{-1})		incident flow	6	12
F	$\frac{U}{hN}$	Froude number	1	6
h_l (m)	$\frac{U}{N}$	gravity height	500	—
F_m	$\frac{U}{h_m N}, \frac{h_l}{h_m}$	mountain Froude number	0.4	6
h_D (m)	$\frac{fL_m}{N}$	deformation depth	300	4000
B	$\frac{h_m N}{fL_m}, \frac{h_m}{h_D}, \frac{\mathrm{Ro}}{F_m}$	Burger number	3.5	0.4
Ro	$\frac{U}{fL_m}$	mountain Rossby number	1.4	2.2
L_m (km)	$\frac{Nh_m}{f}$	mountain Rossby radius	130	20
L_R (km)	$\frac{Nh_m}{f}F_m$	Rossby radius		
	U/f for $F_m < 1$		50	—
	L_m for $F_m > 1$		—	20
ΔV (m s^{-1})	$\frac{N^2h^2}{fL}$, U for $F_m < 1$,	alongshore wind speed change	6	—
	$h_m N$ for $F_m > 1$		—	2

isothermal layer at the freezing level near 850 mb, and near saturation up to about 500 mb. The real-time radar observations from the aircraft suggested bands of convective showers over the ocean, and more continuous stratiform precipitation with embedded convective elements over the windward side of the Olympics. The upstream winds for this case were oriented at about 45° with respect to the longer axis of the near-coast terrain of the Olympic Mountains, but since these mountains are more 3D than 2D, it is unclear what to use for the incipient component of the flow. Nevertheless, it is apparent that the case of 11 December is characterized by a greater onshore velocity and a smaller static stability than the case of 1 December, and hence, a smaller Burger number and a larger Froude number.

4. Flow parameters

The different aspects of the scale analysis for this problem have been discussed previously (Overland 1984; Pierrehumbert and Wyman 1985; Bannon and Chu 1988; Smith 1989; Overland and Bond 1993). The assumptions used in these scale analyses, notably uniform wind speed and static stability under inviscid and adiabatic conditions, are meant to simplify the problem by focusing on the modification of the over ocean wind field by a coastal mountain. Although a more complete numerical simulation study would be possible, our intent is to show that the main functional dependence of the intensity and offshore length scale of coastal jets on stability, onshore wind, and mountain height are demonstrated in the observations and scale analysis.

There are three height scales h one can hypothesize: the mountain height, h_m; the inertial or gravity height scale determined by setting the local Froude number, F, equal to 1, that is, $h_I = U/N$ with notation given in Table 2; and for wide, shallow mountains a deformation depth, $h_D = fL_m/N$. The flow will be semigeostrophic, and the mountain will be hydrodynamically steep if the scaled mountain slope or Burger number $B = h_m/h_D = h_mN/fL_m > 1$. Note that B is also equal to Ro/F_m, where F_m and Ro are the mountain Froude number, $F_m = U/Nh_m$, and mountain Rossby number, $\mathrm{Ro} = U/fL_m$.

If $h_I < h_m$ or likewise $F_m = h_I/h_m < 1$, an appropriate height scale for the disturbance is h_I (Smith 1990). The initial disturbance will grow seaward to a limit given by a Rossby radius L_R based on this height

$$L_R = \frac{Nh}{f} = \frac{Nh_m}{f} F_m = L_m F_m = \frac{U}{f}, \quad F_m < 1. \quad (2a)$$

If $F_m > 1$, however, the mountain height is the appropriate height scale with L_R given by

$$L_R = \frac{Nh_m}{f} = L_m, \quad F_m > 1. \quad (2b)$$

In the case where $F_m \leqslant 1$, the approximate shallow-water gravity wave speed (Nh_I) is equal (and opposite) to the incident wind speed (U), and the seaward extent of the colder air remains fixed. This balance can exist whether the trapped air is due to adiabatic or diabatic cooling of the incident flow, or whether the trapped air has a different source than the incident flow, as in the case of 1 December.

The enhancement in the alongshore wind component is given from the thermal wind relation

$$\Delta V = \frac{g\Delta\theta h}{fL\theta_0} = \frac{N^2h^2}{fL}. \quad (3)$$

Substituting h and L_R into (3) gives

$$\Delta V = U, \quad F_m < 1 \quad (4a)$$

$$\Delta V = Nh_m, \quad F_m \geqslant 1. \quad (4b)$$

It should be noted that these scales are all approximate as spatial changes in stratification, time dependence, and frictional effects modify particular cases.

Results for our December flights are summarized in Table 1. For the Vancouver Island 1 December case $N \sim 0.013\ \mathrm{s}^{-1}$, $U \sim 6\ \mathrm{m\ s}^{-1}$, $h_m \sim 1200$ m, $L_m \sim 40$ km, so $B \sim 3.5$ and $F_m \sim 0.4$. Additionally, $h_I \sim 500$ m in agreement with observations and $L_R \sim 50$ km also in accord with observations. Equation (3) shows that about 6 m s^{-1} of the alongshore wind component of 15 m s^{-1} was due to blocking. Note for moderate winds, L_R in (2) is a function of wind speed. For the North Pacific N is often $O(10^{-2}\ \mathrm{s}^{-1})$ and h_m is $O(1500$ m). Therefore, we expect (2a) and (4a) to roughly hold when $U < 15\ \mathrm{m\ s}^{-1}$.

For the 11 December case with moderate winds but weak stratification, we have an entirely different regime with $F_m \sim 6$. The scale analysis suggests that the ΔV upstream of the terrain should be small, and the modification should occur near the terrain because L_R was only 20 km. The observations are consistent, showing minimal change in the low-level flow from near shore to 60 km upstream. In contrast with the case of 1 December, the wind speeds on 11 December were less near the coast. This change might have been due to synoptic-scale pressure gradient variations, but considering the flow was from the northwest, the terrain-induced pressure perturbations on the western flank of the Olympic Mountains would oppose rather than reinforce the winds at the coast. Given that $0.1 < B < 1$, considerable modification of the wind regime should occur over the coastal slope (Pierrehumbert and Wyman 1985; Xu 1990).

5. Summary

Two cases of onshore flow for overwater winds near coastal orography are investigated using data collected by the NOAA P-3 aircraft in the vicinity of Vancouver Island, British Columbia. Scale analyses suggest that a mountain Froude number, $F_m = U/h_mN$, can be used to characterize the appropriate hydrodynamic regime for scaling the length scales and magnitude of response for the region of blocked flow. In the first case with moderate stratification the near-coast alongshore wind component was increased about 6 m s^{-1} due to blocking; the offshore distance of the modified wind field was 40–50 km. For this case with only a moderate onshore velocity component, the mountain Froude number F_m was less than 1; scale analyses suggest that the offshore length scale of the Rossby radius is given by $L_R = U/f$; that is, the radius of an inertial circle, and the increase in alongshore velocity is $\Delta V = U$. In a second case with a larger onshore velocity and much weaker stratification, the hydrodynamic regime was different with $F_m > 1$, and $\Delta V = h_mN$. Both ΔV and L_R were small for this case. The N of the coastal region can be affected by diabatic processes or by the layering of air masses from different sources, and therefore may not be strictly related to the properties of the incident flow offshore. We expect the largest blocking response and coastal jets would be when $B > 1$ and $F_m \sim 1$; when $F_m < 1$, U is generally small and when $F_m > 1$, N is generally small.

Acknowledgments. This paper was supported in part by the Marine Meteorology Program of the Office of Naval Research as a coastal meteorology project. We thank Aircraft Commander P. Kennedy and his flight

crew for helping to collect outstanding datasets in COAST. Thanks to R. Whitney and P. Quicker for word processing, and K. Birchfield for graphics. PMEL contribution number 1514 and JISAO contribution number 270.

REFERENCES

Bannon, P. R., and P. C. Chu, 1988: An elastic semigeostrophic flow over a mountain ridge. *J. Atmos. Sci.,* **45,** 1020–1029.

Chen, W., and R. B. Smith, 1987: Blocking and deflection of airflow by the Alps. *Mon. Wea. Rev.,* **115,** 2578–2597.

Lackman, G. M., and J. E. Overland, 1989: Atmospheric structure and momentum balance during a gap-wind event in Shelikof Strait, Alaska. *Mon. Wea. Rev.,* **117,** 1818–1833.

Mass, C. F., and G. K. Ferber, 1990: Surface pressure perturbations produced by an isolated mesoscale topographic barrier. Part I: General characteristics and dynamics. *Mon. Wea. Rev.,* **118,** 2579–2596.

Økland, H., 1990: The dynamics of coastal troughs and coastal fronts. *Tellus,* **42A,** 444–462.

Overland, J. E., 1984: Scale analysis of marine winds in straits and along mountainous coasts. *Mon. Wea. Rev.,* **112,** 2530–2534.

——, and N. A. Bond, 1993: The influence of coastal orography: The Yakutat storm. *Mon. Wea. Rev.,* **121,** 1388–1397.

Parish, T. R., 1982: Barrier winds along the Sierra Nevada mountains. *J. Appl. Meteor.,* **21,** 925–930.

Pierrehumbert, R. T., and B. Wyman, 1985: Upstream effects of mesoscale mountains. *J. Atmos. Sci.,* **42,** 977–1003.

Smith, R. B., 1989: Mountain-induced stagnation points in hydrostatic flow. *Tellus,* **41A,** 270–274.

Xu, Q., 1990: A theoretical study of cold air damming. *J. Atmos. Sci.,* **47,** 2969–2985.